Sedimentology (2004) **51,** 767–789 doi: 10.1111/j.1365-3091.2004.00650.x

An experimental investigation of density-stratified inertial gravity currents

C. GLADSTONE*, L. J. RITCHIE†[1], R. S. J. SPARKS‡ and A. W. WOODS*
**BP Institute for Multiphase Flow, University of Cambridge, Cambridge CB3 0EZ, UK (E-mail: lotty@bpi.cam.ac.uk)*
†Centre for Volcanic Studies, University of Luton, Luton LU1 3JU, UK
‡Centre for Environmental and Geophysical Flows, Department of Earth Sciences, University of Bristol, Bristol BS8 1RJ, UK

ABSTRACT

Turbidity currents and pyroclastic density currents may originate as stratified flows or develop stratification during propagation. Analogue, density-stratified laboratory currents are described, using layers of salt solutions with different concentrations and depths to create the initial vertical stratification. The evolving structure of the flow depends on the distribution of the driving buoyancy between the layers, B^* (proportional to the layer volumes and densities), and their density ratio, ρ^*. When the lower layer contains more salt than the upper layer, and so has a greater proportion of the driving buoyancy ($B^* < 0{\cdot}5$), this layer can run ahead leading to streamwise or longitudinal stratification ($\rho^* \to 0$), or the layers can mix to produce a homogeneous current ($\rho^* \to 1$). If the upper layer contains more salt and thus buoyancy ($B^* > 0{\cdot}5$), this layer travels to the nose of the current by mixing into the back of the head along the body/wake density interface to produce a homogeneous flow ($\rho^* \to 1$) or overtaking, leading to streamwise stratification ($\rho^* \to 0$). Timescales describing the mixing between the layers and the streamwise separation of the layers are used to understand these flow behaviours and are in accordance with the experimental observations. Distance–time measurements of the flow front show that strongly stratified flows initially travel faster than weakly stratified flows but, during their later stages, they travel more slowly. In natural flows that are stratified in concentration and grain size, internal features, such as stepwise grading, gradual upward fining and reverse grading, could be produced depending on B^* and ρ^*. Stratification may also be expected to affect interactions with topography and overall fan architecture.

Keywords Inertial gravity current, pyroclastic density current, stratified flow, turbidity current.

INTRODUCTION

Gravity currents are created whenever a density difference between two fluids gives rise to lateral flow of one fluid into another. In many natural turbulent gravity currents of geological importance, the density difference between the propagating current and the ambient fluid is the result of suspended particulate matter as well as fluid of different composition and hence density. Particle-driven gravity currents are important in many geological and environmental settings in terms of sediment transport and dispersal (Simpson, 1997; Mulder & Alexander, 2001). Particulate gravity currents can also have considerable destructive potential. For example,

[1]Present address: Shell International Exploration and Production, Inc., 200 North Dairy Ashford, Houston, TX 77079, USA.

pyroclastic flows and snow avalanches represent a significant hazard (Hopfinger, 1983; Druitt, 1998), and thus insights into the flow dynamics and deposition from turbulent gravity currents is important for risk assessment near volcanoes and in populated alpine areas. To increase recovery rates of hydrocarbons held in the deposits of turbidity currents, understanding of their parent flows and the processes that generated the deposits is required. The infrequent occurrence and highly destructive nature of these events limit the number of detailed observations of natural flows. In particular, the lack of direct observational data for submarine events is acute, because of their infrequency and inaccessible location. For these reasons, laboratory experiments and theoretical analyses play an important role in furthering understanding of natural gravity currents.

Experimental and theoretical studies of high Reynolds number gravity currents have mainly focused on flows that develop from initially homogeneous mixtures (e.g. Middleton, 1966; Huppert & Simpson, 1980; Hallworth *et al.*, 1996). However, in vertical section, the deposits of both pyroclastic density currents and turbidity currents commonly show strong particle segregation into characteristic zones divided by grain-size discontinuities (Druitt, 1998; Clayton, 1994; Sinclair, 1994), and flow stratification has been invoked as a possible dynamical explanation for such features (Gladstone & Sparks, 2002; Ritchie *et al.*, 2002). There are many situations in which natural currents may become vertically stratified in terms of grain size and sediment concentration, owing to the initial source conditions or processes in the flow. For example, stratification can arise from the variable settling velocities of different particle sizes, variations in turbulence intensity within the flow (Kneller & Buckee, 2000; Buckee *et al.*, 2001), entrainment of air or water at the margins of the flow (Hallworth *et al.*, 1996) and entrainment of sediment from the underlying substrate. An additional mechanism that can promote stratification is present in volcanic settings if a pressurized dome decompresses explosively to release a suspension into the air, which can stratify in grain size and concentration before collapsing to form a turbulent pyroclastic density current (Ritchie *et al.*, 2002; Woods *et al.*, 2002).

The purpose of the present paper is to examine the dynamics of stratified gravity currents through a series of simple laboratory experiments. A suite of systematic two- and three-layer density-stratified gravity currents is described, and results and interpretations are presented on the effect of some of these key features, with implications for sediment deposition from particle-laden gravity currents. In these experiments, the fractional depths and density of each layer are varied using salt solutions of varying concentration, and the position of the current nose is measured, with flow visualization using dyes that allow assessment of the interactions between layers. Four series of experiments are presented, each exploring a specific aspect of the problem (Fig. 1 and Table 1); series A investigates the effect of lower layer depth on the dynamics of the flow; series B investigates two-layered currents where the lower layer contains more salt, and therefore has a greater driving buoyancy, than the upper layer; series C investigates two-layered currents in which the lower layer contains less salt and thus less driving buoyancy than the upper layer; series D studies three-layered currents with varying strengths of stratification, while keeping the total current density constant. These inertial, density-stratified experiments allow the roles of both the density difference and the distribution of buoyancy between the layers on the behaviour of the flow to be assessed.

THEORETICAL CONTEXT

Early investigations of inertial gravity currents were carried out by Schmidt (1911), von Karman (1940) and Keulegan (1957) who released fixed volumes of saline water into freshwater channels and documented advance of the flow front. The evolution of gravity current morphology as a function of time was studied by Middleton (1966) and considered experimentally and theoretically by Huppert & Simpson (1980). Reviews of experimental work in this field are provided by Middleton (1993) and Kneller & Buckee (2000).

After an initial gravitational collapse out of the lock, these types of saline flows are driven by a balance of inertial and buoyancy forces, where frictional resistance is considered to be unimportant and, therefore, the speed of the flow, u, must be a function of the two-dimensional driving buoyancy of the fluid, B, and a lengthscale that is taken as L. From dimensional considerations, these parameters combine to give

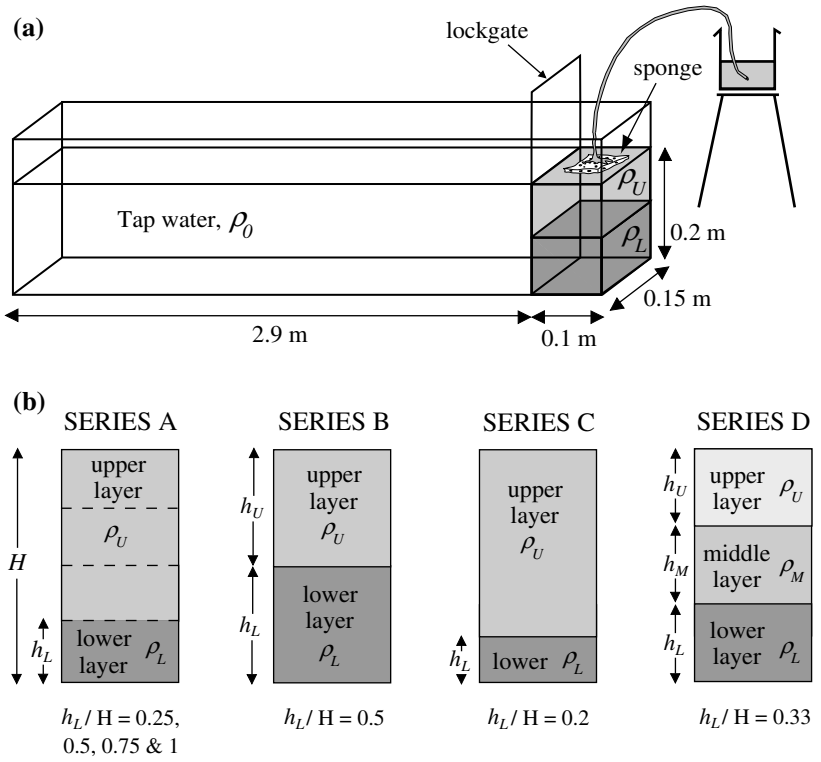

Fig. 1. (a) Arrangement of layers of different density for each of the four experimental series. In series A–C, two layers were placed in the lock region, a lower dense layer of depth h_L and density ρ_L, overlain by an upper layer of depth h_U and density ρ_U. For series D, a third layer of density and depth ρ_M and h_M was added. (b) Schematic diagram of experimental apparatus showing emplacement of the two-layer stratification through a floating sponge. In all experiments the ambient fluid was fresh water at $\approx$16·5 °C so $\rho_0 = 998{\cdot}9$ kg m^{-3}.

$$u \sim \left(\frac{B}{L}\right)^{1/2} \tag{1}$$

The buoyancy of a two-dimensional flow has units $[L^3/T^2]$ and is defined as

$$B = Ag' \text{ where } g' = g(\rho_C - \rho_0)/\rho_0 \tag{2}$$

and A is the two-dimensional area of the current, g the acceleration due to gravity, and ρ_C and ρ_0 the densities of the current and ambient fluid respectively. Note that, during propagation, both ρ_C and A may be changing, but the total driving buoyancy B will remain constant because it is equal to the mass of salt used to create the flow, which must be conserved. Therefore, at all times,

$$B = B_0 = A_0 g_0' \tag{3}$$

where the subscript zero denotes initial values. Substituting Eq. (3) into Eq. (1) gives

$$u = \frac{dL}{dt} = Fr\left(\frac{A_0 g_0'}{L}\right)^{1/2} \tag{4}$$

where the Froude number, Fr, is a scaling constant. Benjamin's (1968) analysis of gravity current propagation identified a theoretical value for the Froude number of $\sqrt{2}$. A slightly lower value of 1·19 is appropriate for laboratory gravity currents using the lock-exchange technique, when the current is thin compared with the ambient depth (Huppert & Simpson, 1980).

Eq. (4) can be integrated to provide a description of the position of the flow front, L, with time, t,

$$L^{3/2} = L_0^{3/2} + 2/3Fr(A_0 g_0')^{1/2} t \tag{5}$$

where L_0 is the length of the lock, i.e. the initial length of the flow at time $t = 0$. This scaling has been shown to describe homogeneous saline and simple particle-laden currents in the laboratory reasonably well (Huppert & Simpson, 1980; Bonnecaze *et al.*, 1993; Dade & Huppert, 1995; Gladstone & Woods, 2000). Eq. (5) can be written in dimensionless terms by introducing the dimensionless distance travelled by the current, L^*, with dimensionless time, t^*,

$$L^{*3/2} = 1 + t^* \tag{6}$$

Here,

$$L^* = L/L_0 \tag{7}$$

and

Table 1. Initial conditions for all experiments.

Experiment	ρ_C	ρ_L	ρ_U	h_L/H	ρ^*	B^*
Series A: effect of lower layer depth						
A1*	1013·9	998·9	1061·8	0·25	0	0
A2	1013·9	998·9	1029·7	0·5	0	0
A3	1013·9	998·9	1018·9	0·75	0	0
A4	1013·9	998·9	1013·9	1	0	0
Series B: more driving buoyancy in the lower layer so $B^* < 0{\cdot}5$						
B1	1070·7	1078·1	1063·3	0·5	0·81	0·45
B2	1070·7	1085·7	1055·9	0·5	0·66	0·40
B3	1070·7	1093·2	1048·6	0·5	0·53	0·35
B4	1070·7	1100·8	1041·3	0·5	0·42	0·29
B5*	1070·7	1108·5	1034·0	0·5	0·32	0·24
B6	1070·7	1116·2	1026·8	0·5	0·24	0·19
B7*	1070·7	1124·0	1019·6	0·5	0·17	0·14
B8	1070·7	1131·9	1012·5	0·5	0·10	0·09
B9	1070·7	1139·8	1005·3	0·5	0·05	0·04
B10*	1070·7	1070·7	1070·7	0·5	1·00	0·50
B11*	1012·5	1012·5	1012·5	0·5	1·00	0·50
B12*	1012·5	1019·6	1005·3	0·5	0·31	0·24
B13	1012·9	1026·8	998·9	0·5	0·00	0·00
B14*	1016·0	1019·5	1012·5	0·5	0·66	0·40
B15	1016·1	1026·8	1005·3	0·5	0·23	0·19
B16	1016·1	1016·1	1016·1	0·5	1·00	0·50
B17*	1016·5	1034·0	998·9	0·5	0·00	0·00
B18	1021·5	1034·0	1008·9	0·5	0·28	0·22
B19	1023·3	1034·0	1012·5	0·5	0·39	0·28
B20	1025·0	1034·0	1016·0	0·5	0·49	0·33
B21	1026·8	1034·0	1019·6	0·5	0·59	0·37
B22	1028·6	1034·0	1023·2	0·5	0·69	0·41
B23	1030·4	1034·0	1026·8	0·5	0·79	0·44
B24	1032·2	1034·0	1030·4	0·5	0·90	0·47
B25	1014·0	1026·1	1001·8	0·5	0·11	0·10
B26	1013·9	1018·2	1009·6	0·5	0·55	0·36
B27	1011·0	1034·0	1005·3	0·2	0·18	0·42
B28	1015·2	1034·0	1008·9	0·25	0·28	0·46
B29	1030·4	1034·0	1019·6	0·75	0·59	0·16
B30	1009·9	1034·0	998·9	0·3	0·00	0·00
Series C: more driving buoyancy in the upper layer so $B^* > 0{\cdot}5$						
C1	1014·1	1017·5	1013·2	0·2	0·77	0·75
C2	1008·2	1034·0	1005·3	0·1	0·18	0·62
C3	1009·2	1034·0	1005·3	0·15	0·18	0·51
C4	1013·9	1034·0	1008·9	0·2	0·28	0·53
C5	1016·8	1034·0	1012·5	0·2	0·39	0·61
C6	1019·6	1034·0	1016·0	0·2	0·49	0·66
C7	1028·2	1034·0	1026·8	0·2	0·79	0·76
C8	1017·9	1034·0	1012·5	0·25	0·39	0·54
Series D: three-layer currents						
D1	1017·3	1044·9	1005·3	1001·8	0·14	0·45
D2	1017·3	1026·8	1023·2	1001·8	0·87	0·12
D3	1017·3	1023·2	1016·0	1012·5	0·70	0·80

Four series were conducted, each investigating a different aspect of density-stratified inertial flows. Experiments B1–B10 were carried out in a 6 m tank; all others were performed in a 3 m tank. The variables are: density of the total current, ρ_C; lower layer, ρ_L; upper layer, ρ_U; and in three-layer experiments of series D, the density of the middle layer, ρ_M, in kg m^{-3}; the fractional depth of the lower layer is given by h_L/H. A dimensionless density ratio, ρ^*, and dimensionless buoyancy distribution, B^*, between the layers are defined in Eqs (10) and (11). Experiments marked with an asterisk were run two to four times to assess reproducibility.

$$t^* = t/\tau \quad (8)$$

where $\tau = 1/[2/3Fr(A_0 g'_0)^{1/2} L_0^{-3/2}]$

These scalings are used throughout the present paper to collapse experimental data and identify those flows within the inertial regime and those where drag has become an important control.

Little is known about the effects of density stratification in such flows, even though there is field evidence that stratified currents may occur in nature (e.g. Kneller & McCaffrey, 1999; Stix, 2001). In the present paper, the dynamics of experimental gravity currents that have been initiated from stratified source conditions are examined. A variety of behaviours can be envisaged as a result of differing initial conditions. For two-layered currents, it can be inferred from Eq. (1) that, in the absence of interaction between the layers, the layer with the highest buoyancy will propagate ahead of the less dense fluid. Initial strong vertical stratification would thus result in pronounced streamwise stratification of the flow, with the lower denser part of the current running ahead of the upper, less dense part. However, mixing of the flow could occur during propagation if the density contrast between layers is small; in this case, the layers can no longer be considered as separate components of the flow. A further complication may arise in a flow with a thin lower layer where the effect of friction may suppress the development of the streamwise stratification. The object of this research is thus to investigate, through systematic experiments and simple scalings, the details of each behaviour and assess the initial conditions under which these develop.

EXPERIMENTAL METHOD

Experiments were conducted in one of two tanks. The first was an acrylic tank, 3 m long and 0·15 m wide, filled with tap water to a depth of 0·2 m (Fig. 1a). A watertight lockgate was situated 0·1 m from one end of the tank. Most experiments presented here were conducted in this tank. The second tank was glass with a length of 5 m, width 0·2 m, with a gate placed 0·2 m from the end wall and filled to a depth of 0·4 m. Aqueous saline solutions were prepared using varying masses of NaCl to produce a known excess density. In each experiment, the temperature of the ambient fluid and saline solutions in the lock region were held constant so that the density difference between the current and ambient fluid was solely due to compositional variations, not temperature variations. However, slight temperature variations between one experiment and the next, due to seasonal variations in tap water temperature, produced a temperature range of 15 °C ($\rho_0 = 999{\cdot}1$ kg m^3) to 17·5 °C ($\rho_0 = 998{\cdot}7$ kg m^3). The density change caused by this temperature range is very small compared with that produced by salt solutions (Table 1), and so all fluids are treated as being at a constant temperature of 16·5 °C ($\rho_0 = 998{\cdot}9$ kg m^3).

For series A–C, two layers of different density and depth were placed behind the lockgate with the densest solution forming the lower layer (Fig. 1a and b). The upper layer was emplaced through a sponge to reduce the effects of turbulent mixing between the two layers during set-up. For the three-layer experiments of series D, the process was repeated to emplace the top layer (Fig. 1b). Typically, a mixed region of depth 2–4 mm formed between the layers. The role of this region on the dynamics of the flow is considered to be unimportant, because the depth of the mixed region is small compared with the total depth of the lock, and mixing of the layers through molecular diffusion is negligible over the set-up time of the experiment. This was validated through repeated experiments (see below). Solutions were coloured with 1 mL of blue, yellow or red food dye per 1 L of saline solution to allow the layers to be distinguished and the onset of mixing to be visualized. The lockgate was then lifted to release the layered solutions into the main tank.

The position of the flow front, L, was measured every 3 s after release by marking the position of the frontmost lobe of the flow on the tank during the experiments. Measurements continued until the currents became too dilute to distinguish from the ambient fluid or reflection from the end of the flume tank occurred. Non-systematic errors were assessed through multiple runs of the same experiment; 3% error bars are plotted on the four repeated experiments of B12 to illustrate the good reproducibility (Fig. 2). Close to the end of the tank, the presence of the endwall impacts on the flow, and so data taken within 50 cm of this are discarded. Colour photographs were taken using a Nikon digital still camera at constant time intervals of 4 s to allow the interactions between layers to be assessed through mixing of the blue and yellow dyes. For additional clarity, the experiment was backlit using three parallel light sources placed 2·4 m behind the tank, with a single sheet of tracing paper along the front of the

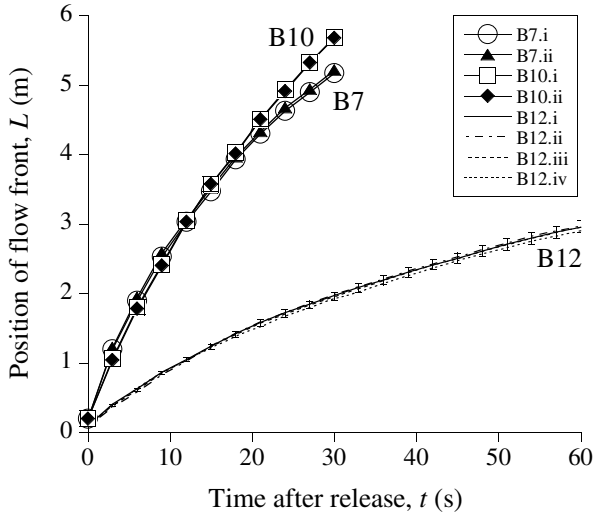

Fig. 2. Multiple runs of three different experiments show that the reproducibility of distance–time data is within ±3%, indicated by error bars plotted with the data gathered from four runs of B12. To cover a range of initial conditions, the three selected experiments are B7 (strong stratification, 6 m tank), B10 (no stratification, 6 m tank) and B12 (medium stratification, 3 m tank). Details of each are given in Table 1.

tank. The light passing through the tank projects planes of different refractive index on to the paper in the foreground, providing visualization of width-averaged regions with density contrasts. This 'shadowgraph' technique is particularly useful for picking out mixing between fluids with different densities. However, when using multiple light sources to illuminate large areas such as the flume tank used in these experiments, 'false' shadows can occasionally appear (for example, at the nose of the flow in the second frame of Figs 3a and 9a). Although every effort was made to minimize these effects, it was not possible to remove them entirely.

Here, the subscripts L and U refer to lower layer and upper layer respectively. For two-layer experiments, the lock region was filled with a lower layer of depth h_L and density ρ_L created using a mass of salt M_L, and a less dense upper layer of depth h_U, density ρ_U and salt mass M_U, so that the total depth of lock fluid ($h_L + h_U$) equalled the depth of ambient fluid in the main section of the tank, H (Fig. 1b). Thus, the bulk density of the current, ρ_C, is given by

$$\rho_C = (h_L\rho_L + h_U\rho_U)/H \tag{9}$$

Note that the phrase 'mass of salt' is quite distinct from salinity. The mass of salt reflects the product of layer density and layer depth and is therefore proportional to the two-dimensional driving buoyancy, whereas salinity is directly proportional to density. Thus, the term salinity is deliberately not used in this paper.

In order to allow direct comparison between flows created using a variety of different initial conditions, it is useful to define a dimensionless density ratio between the layers, ρ^*, and dimensionless difference in the driving buoyancy, B^*, where

$$\rho^* = \frac{\rho_U - \rho_0}{\rho_L - \rho_0} = \frac{g'_U}{g'_L} \tag{10}$$

and

$$B^* = \frac{B_U}{B_U + B_L} = \frac{h_U g'_U}{(h_U g'_U + h_L g'_L)} \equiv \frac{M_U}{M_U + M_L} \tag{11}$$

The ratio ρ^* quantifies the strength of the initial stratification: a small value of ρ^* indicates a strong stratification; as $\rho^* \to 1$, the stratification becomes weaker and, at $\rho^* = 1$, there is no stratification and the flow is homogeneous. At $\rho^* = 0$, all the current density is contained in the lower layer and, thus, the upper layer and ambient fluid have equal densities. Similarly, at $B^* = 0$, all the salt is placed in the lower layer and $\rho_U = \rho_0$. Values of $0 < B^* < 0{\cdot}5$ indicate that more of the salt is contained in the lower layer than in the upper layer. When $B^* = 0{\cdot}5$, the salt is evenly distributed between the layers, and so the buoyancy contribution by each layer to the gravity current is equal. Values of $1 > B^* > 0{\cdot}5$ indicate that more salt is contained in the upper layer, which is achieved in the laboratory by increasing the fractional depth of the upper layer.

For this particular study, 46 experiments were conducted with experimental conditions given in Table 1, covering a wide range of values of ρ^* (0–1) and B^* (0–0·76). A further 14 multiple experiments were run to assess reproducibility. The currents photographed in Figs 3d, 5 and 9 were arranged with the same bulk density, $\rho_C = 1014$ kg m^{-3}, to

Fig. 3. Photographs at different time intervals illustrate the flow of gravity currents where the height of the lower layer is varied. A constant mass of salt is added to the lower layer (0·066 kg), and the upper layer is composed of fresh tap water in each experiment. The bulk current density (combining both layers) is $\rho_C = 1014$ kg m^{-3}. (a) $h_L/H = 0{\cdot}25$. (b) $h_L/H = 0{\cdot}5$. (c) $h_L/H = 0{\cdot}75$. (c) $h_L/H = 1{\cdot}0$. The photographs reveal that an initially small lower layer can lead to rapid thinning of the flow, while an initially larger lower layer can cause thickening of the flow.

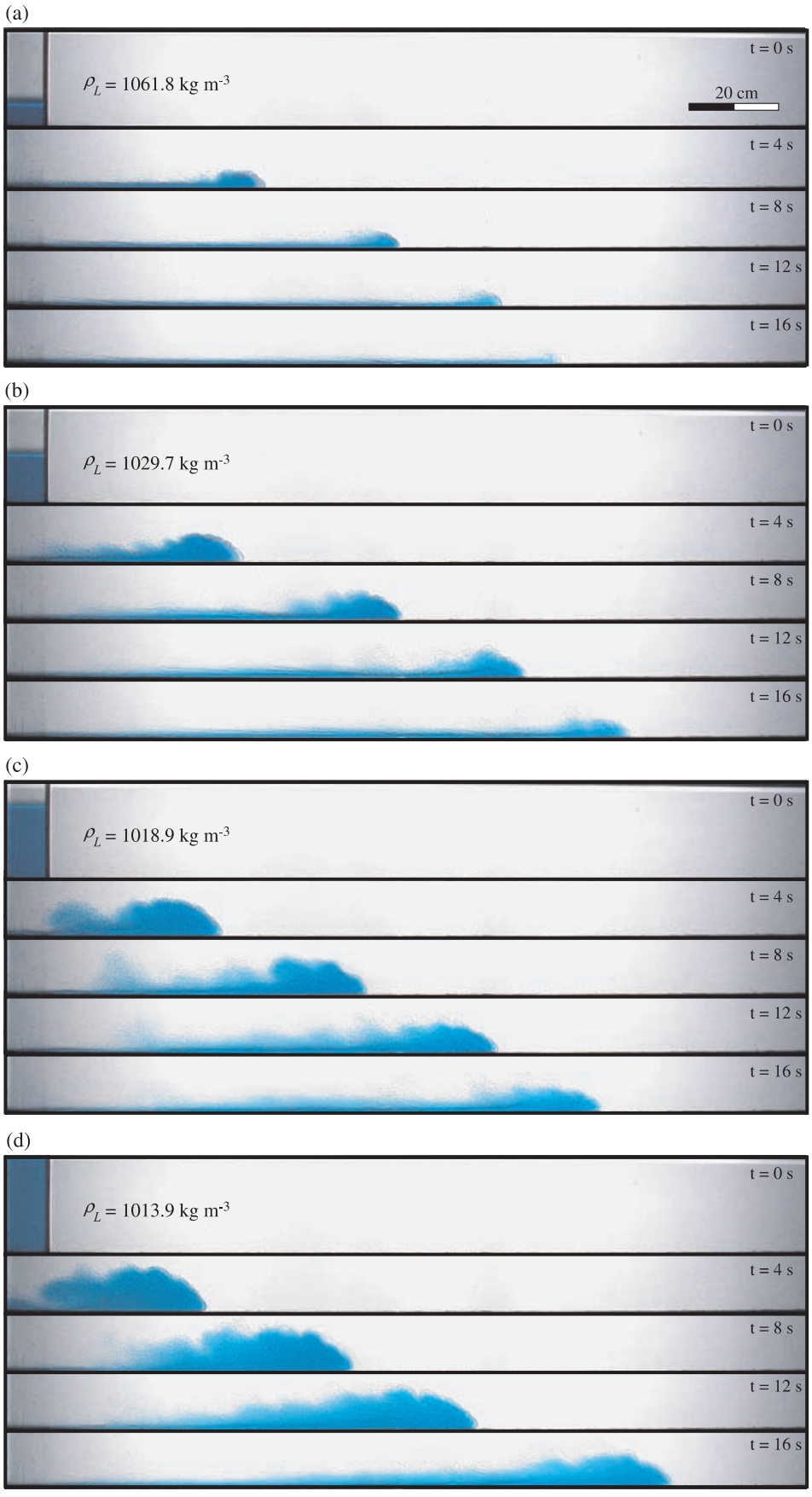
(a)
ρ_L = 1061.8 kg m^{-3}
20 cm
t = 0 s
t = 4 s
t = 8 s
t = 12 s
t = 16 s
(b)
ρ_L = 1029.7 kg m^{-3}
t = 0 s
t = 4 s
t = 8 s
t = 12 s
t = 16 s
(c)
ρ_L = 1018.9 kg m^{-3}
t = 0 s
t = 4 s
t = 8 s
t = 12 s
t = 16 s
(d)
ρ_L = 1013.9 kg m^{-3}
t = 0 s
t = 4 s
t = 8 s
t = 12 s
t = 16 s

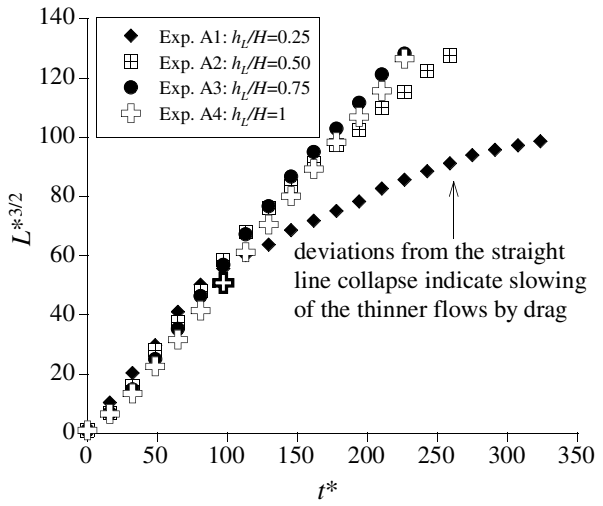

Fig. 4. The dimensionless distance reached by the flow front, $L^{*3/2}$, at different dimensionless times, t^*, is plotted for the flows from series A, which are photographed in Fig. 3. The thinner flows deviate from a straight-line collapse, indicating that frictional or viscous effects are retarding these flows, and they are no longer purely inertial. Flows with an initially thicker lower layer collapse well, indicating that they remain inertial over the duration of the experiment. Each experiment is identified by a letter and a number; initial conditions are listed in Table 1.

aid comparisons of flow behaviour. Typical Reynolds numbers during the time considered in the photographs range from 7000 down to 3000, although at later times and distances, the Reynolds number of the thinnest currents decreases to 800–1000. The experimental flows are characterized by an approximately constant Froude number of 1·3. The method used for estimating these values and their implications is given in more detail in the discussion on the application of these small-scale flows to full-scale natural turbidity currents and pyroclastic density currents.

EXPERIMENTAL RESULTS

Series A: effect of lower layer depth

The first series of experiments, series A (Fig. 1b), was conducted to investigate the effects of drag on a single-layer current by varying the depth of the lower layer of saline fluid but keeping the total mass of salt, and thus $\rho_C H$, constant (cf. Huppert & Simpson, 1980; Hogg & Woods, 2001). The stratification in the lock was arranged with a lower layer containing 0·066 kg of NaCl and an upper layer and main tank ambient fluid of fresh water. The lower layer depth was varied in each experiment so that $h_L/H = 1$, 0·75, 0·5 and 0·25 (Fig. 1b; Table 1). For each of the four experiments, photographs are presented to assess the overall characteristics of the currents (Fig. 3), and collapsed distance–time data using the simple scalings given by dimensional analysis in Eqs (7) and (8) are plotted in Fig. 4.

Photographs show that, when the current has a small initial height, there is less mixing with the ambient fluid and the flow thins rapidly (Expt A1, Table 1; Fig. 3a). Corresponding scaled distance–time data that have been non-dimensionalized using Eqs (7) and (8) illustrate that the initial slump of thin flows ($h_L/H \leq 0{\cdot}5$; Expts A1 and A2) is slightly faster than that of thicker flows. A large (ρ_L–ρ_0) leads to a fast flow; during the early slump phase, the thin dense lower layer causes the nose of the current to flow quickly. However, these thin flows dissipate, and frictional effects become important, causing the flows to decelerate rapidly. This is clear from Fig. 4 where flow A2 ($h_L/H = 0{\cdot}5$) deviates slightly from the straight-line collapse towards the end of the experiment, while the thinnest flow, A1 ($h_L/H = 0{\cdot}25$), deviates from the line earlier, indicating that the effects of drag are important in retarding the flow for much of the experiment.

For thicker currents where $h_L/H > 0{\cdot}5$, the velocity of the initial slump is slightly less than the thin flows because ρ_L–ρ_0 is smaller. Subsequently, the current advances more rapidly as it is sufficiently deep and therefore less affected by friction (Figs 3c and d and 4). For flows A3 and A4, where $h_L/H = 0{\cdot}75$ and 1, and much of A2 ($h_L/H = 0{\cdot}5$), the simple scalings are appropriate as shown by the straight-line collapse of the dimensionless data. This indicates that, over the experimental duration, the flow is controlled by a balance between inertial and buoyancy forces, and drag is not important.

Series B, $B^* < 0{\cdot}5$: driving buoyancy of lower layer < driving buoyancy of upper layer

In series B experiments, the effects of stratification were examined in currents in which the lower layer contained a larger mass of salt than the upper layer, i.e. $\rho_L h_L > \rho_U h_U$. In the experiments presented, the initial depth of each layer was equal, $h_L = h_U$ (Figs 1b and 5), but the density contrast between the two layers, ρ^*, was varied with the bulk current density being kept constant (Table 1). Although the distribution of

buoyancy between the layers was varied throughout the series, in all experiments $B^* < 0{\cdot}5$.

With a large density contrast between the layers ($\rho^* = 0{\cdot}11$), the lower layer surges ahead of the upper layer, forming a gravity current consisting of a bulbous head with a turbulent wake and a body (Fig. 5a). As the upper layer is considerably less dense than the lower layer, it is unable to catch the front of the current but can be seen to intrude into the body of the lower layer as a thin wedge (Fig. 5a, Expt B25). Mixing between the two layers is minimal, although a small region of green mixed fluid can be seen immediately above and below the intruding wedge. Eventually, the lower layer slows sufficiently to allow the upper layer gradually to catch up. When the density contrast between the layers is small ($\rho^* = 0{\cdot}55$), the upper layer intrudes quickly between the dilute turbulent wake and the denser, main part of the flow of the lower layer (Fig. 5b, Expt B26). The layers mix rapidly as upper layer fluid intruding into the back of the flow head is stripped away by ambient entrainment and passed into the overlying turbulent wake.

Plots of flow front velocity with time indicate that a strongly stratified flow travels most rapidly during the initial stages of the current (0–6 s; Fig. 6a), because the lower layer that is driving the flow during this part of the experiment has a higher density contrast with the ambient fluid than a weakly stratified flow. However, the velocity of the strongly stratified flow declines rapidly because the upper layer, which has the smallest density contrast with the ambient fluid, is being left behind and is thus not contributing to the velocity of the flow front. By considering the scaled distance–time data, it is possible to identify when the effects of drag begin to contribute to this velocity decrease. The good straight-line collapse before $t^* = 200$ suggests that, up to this point, the flow is inertial (Fig. 6b). By $t^* = 200$, however, the scaled data are deviating from the straight line, indicating that the flow is no longer purely inertial and drag is also now important (Fig. 6b; compare with previous section on effect of lower layer depth).

The velocity variations can be assessed further by normalizing the distance–time data to a calibration homogeneous flow. In Fig. 6c, the distance reached at each time, *L(t)*, by flows with the same bulk current density of 1070·7 kg m^{-3} is divided by the distance reached at the same time by a homogeneous flow with the same initial density, *X(t)*. This plot accentuates the velocity differences, verifying that, with a strong initial stratification, the dense lower layer dominates to drive the flow at a higher velocity than a weakly stratified current (e.g. $\rho^* = 0{\cdot}05$, Expt B9). However, the velocity deceleration is greater and thus the flow is slower during later stages, compared with a flow with a weaker initial stratification ($\rho^* = 0{\cdot}81$, Expt B1).

Series C, $B^* > 0{\cdot}5$: driving buoyancy of upper layer > driving buoyancy of lower layer

Series C was conducted to investigate the propagation of stratified flows in which the upper layer contains a greater mass of salt than the lower layer, $\rho_U h_U > \rho_L h_L$, achieved experimentally by reducing h_L and increasing h_U. In all experiments (Figs 7 and 8), the lower layer initially propagated to form the nose of the current, but was quickly caught up by the upper layer. However, the density contrast, or degree of stratification, governs the way in which the upper layer reaches the front of the flow and the amount of mixing occurring between the two layers. For the photographs in Fig. 7, the depth of the lower layer was kept constant at $h_L/H = 0{\cdot}2$ as was the total mass of salt behind the lockgate, $M_U + M_L$, and thus the bulk density $\rho_C = 1014$ kg m^{-3}. By distributing the salt differently between the two layers, this yielded strong (Fig. 7a, $\rho^* = 0{\cdot}28$, Expt C4) and weak stratification (Fig. 7b, $\rho^* = 0{\cdot}77$, Expt C1).

When the density contrast between the two layers is large, the upper layer moves to the flow front by intruding into the lower layer as a thin wedge below the developing, less dense turbulent wake of the lower layer (Fig. 7a). Some of the upper layer mixes into the wake as it runs through and ahead of the lower layer. This results in vertical stratification of the fluid with a lower region of dense fluid (blue), a middle layer of less dense fluid (yellow) and an upper mixed region composed of fluid from both upper and lower layers (green; Fig. 7a). As this green region is uppermost, it has the smallest density, indicating that it has been diluted by entrainment of ambient fluid with density ρ_0. In contrast, when the density contrast between the layers is small, the intrusion of the upper layer fluid into the advancing lower layer is rapid and the two layers mix (Fig. 7b). The upper layer does not over-ride the lower layer but intrudes below a region of diluted fluid from the head of the lower layer. The velocity of the current for these two flows is very similar. Both

(a)

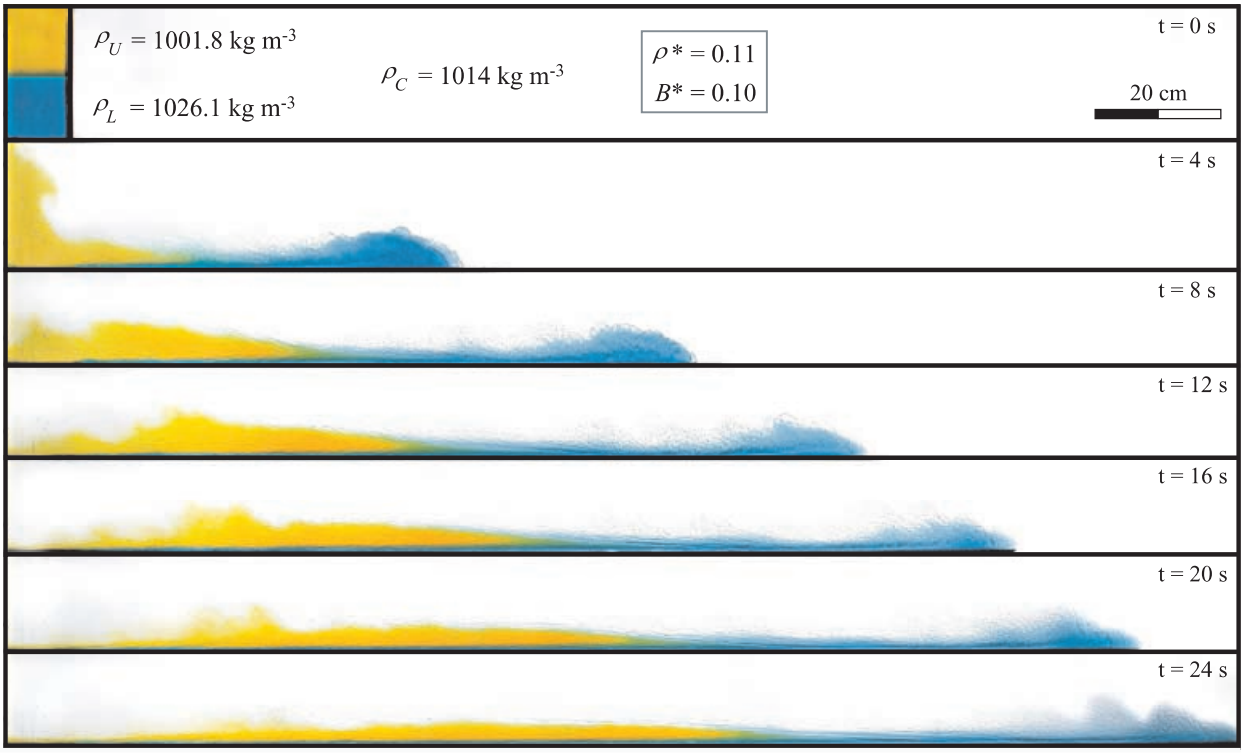

(b)

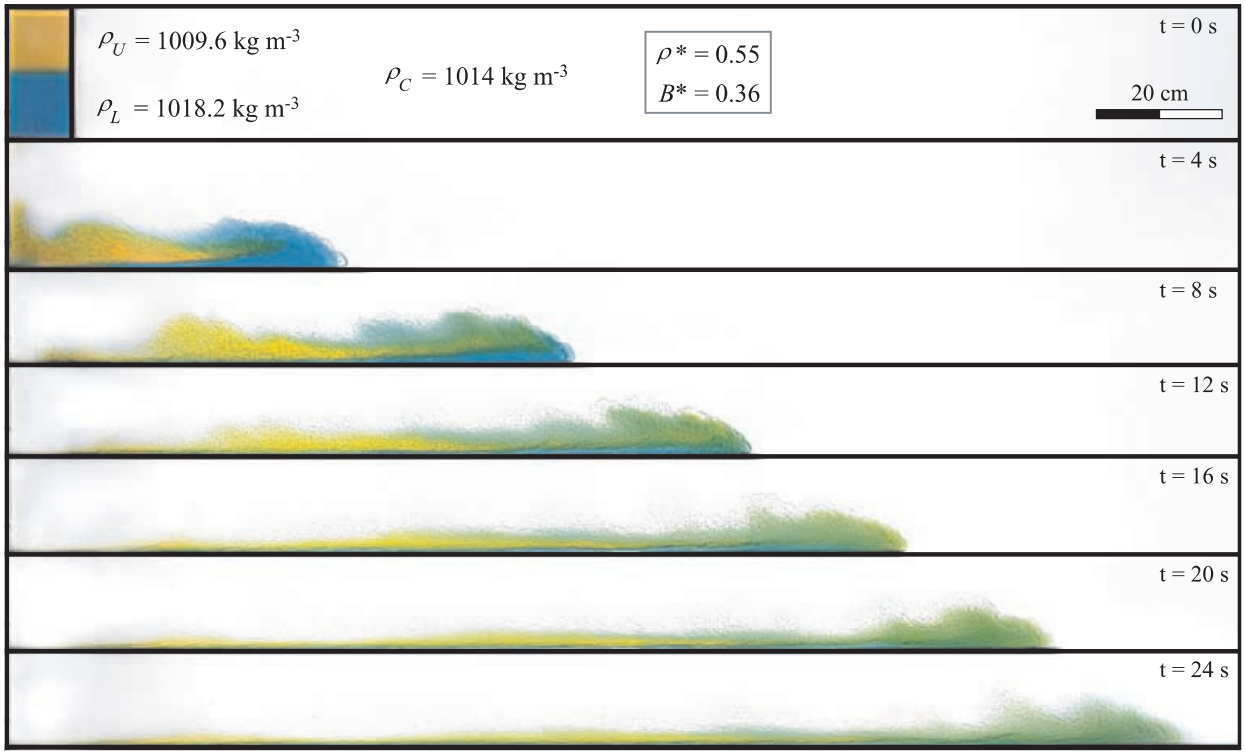

distance–time data sets collapse well using the scalings for an inertial saline current, showing that, although the lower layer is initially thin, due to the mixing and dilution of the flow, friction does not cause the deceleration of either flow (Fig. 8).

Fig. 5. Photographs depicting the development of two flows from series B, where the mass of salt in the upper layer, M_U, is less than that in the lower layer, M_L (i.e. $\rho_U h_U < \rho_L h_L$), so the lower layer contains more of the driving buoyancy, $B^* < 0{\cdot}5$. (a) An initially strongly stratified current propagates forward (Expt B25). The lower layer runs ahead to drive the flow while the upper layer is left behind. (b) Here, the current is initially weakly stratified and the two layers mix rapidly (Expt B26). Both flows have the same initial bulk current density, $\rho_C = 1014$ kg m^{-3}.

Series D: three-layer density-stratified currents

The previous sets of experiments have identified that two-layer currents may decouple or mix, depending on the density ratio and the distribution of driving buoyancy between the layers. This approach was extended to three-layer density-stratified laboratory currents in series D (Table 1) to assess whether these observations are applicable to flows of more variable stratification. For these three flows, the depth of each layer was the same so $h_L = h_M = h_U$, and the total bulk density of each current was kept constant at $\rho_C = 1017$ kg m^{-3} (Figs 1b and 9). The density contrast between the layers was varied from strongly stratified (Expt D1) to a nearly homogeneous flow (Expt D3). For each flow, colour photographs are presented in Fig. 9 and scaled distance–time data using Eqs (7) and (8) in Fig. 10.

When the lower layer contains most of the driving buoyancy, it runs ahead of the upper two layers but is affected by friction and thins rapidly (Figs 9a and 10). When close in density, the upper two layers mix rapidly and do not immediately catch up with the lower layer, but intrude into the body of the lower layer current as a thin wedge below a diffuse mixed zone (Fig. 9a). When the lower two layers are of

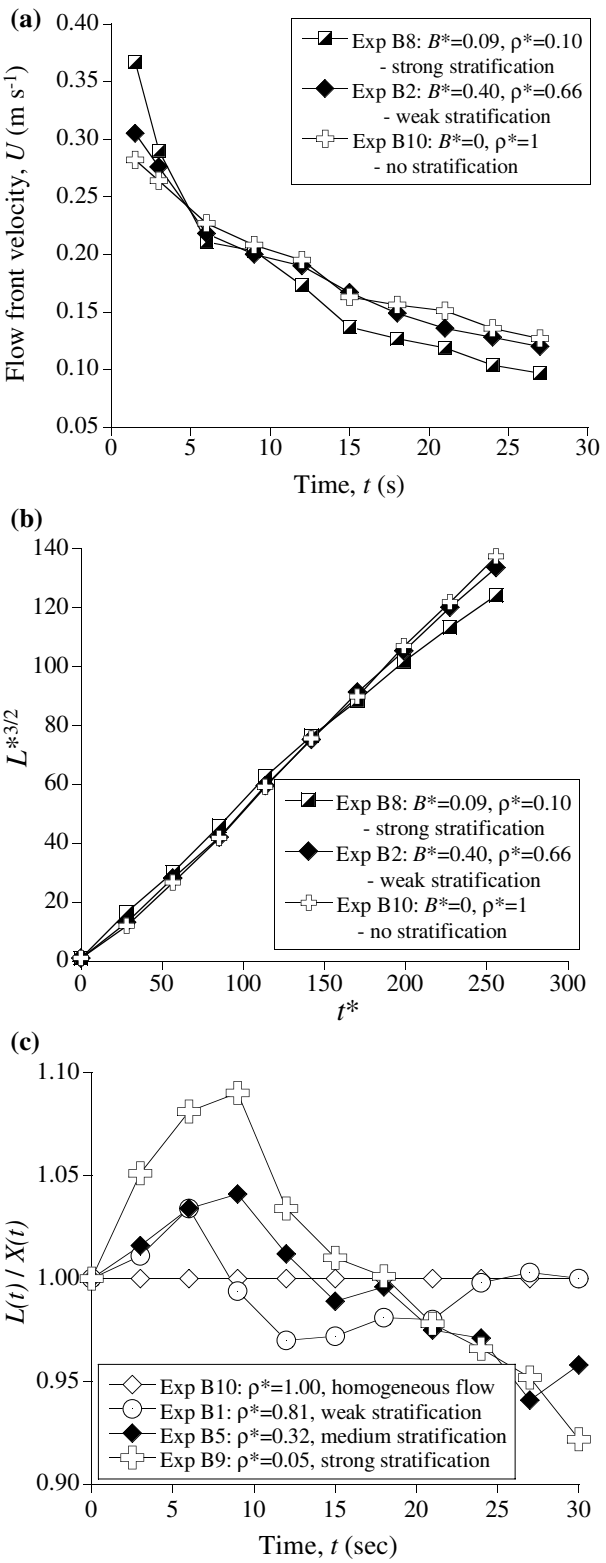

Fig. 6. (a) The decrease in flow front velocity, u, with time, t, is plotted for three flows with the same total density ρ_C: a homogeneous flow (B10), a weakly stratified flow (B2) and a strongly stratified flow (B8). Compared with a homogeneous current, the strongly stratified flow travels faster during early stages but slower during later stages. (b) Using the scalings given in Eqs (7) and (8) shows that these flows collapse well to a straight line and so are largely inertial, although the deviation of the data from the strongly stratified flow, B8, during later stages indicates the onset of viscous effects. (c) The distance reached by a stratified flow at each time interval, $L(t)$, is normalized on the distance reached by its homogeneous counterpart with the same bulk density, $X(t)$. This verifies that density-stratified flows travel faster during early stages but slower during later stages than well-mixed flows.

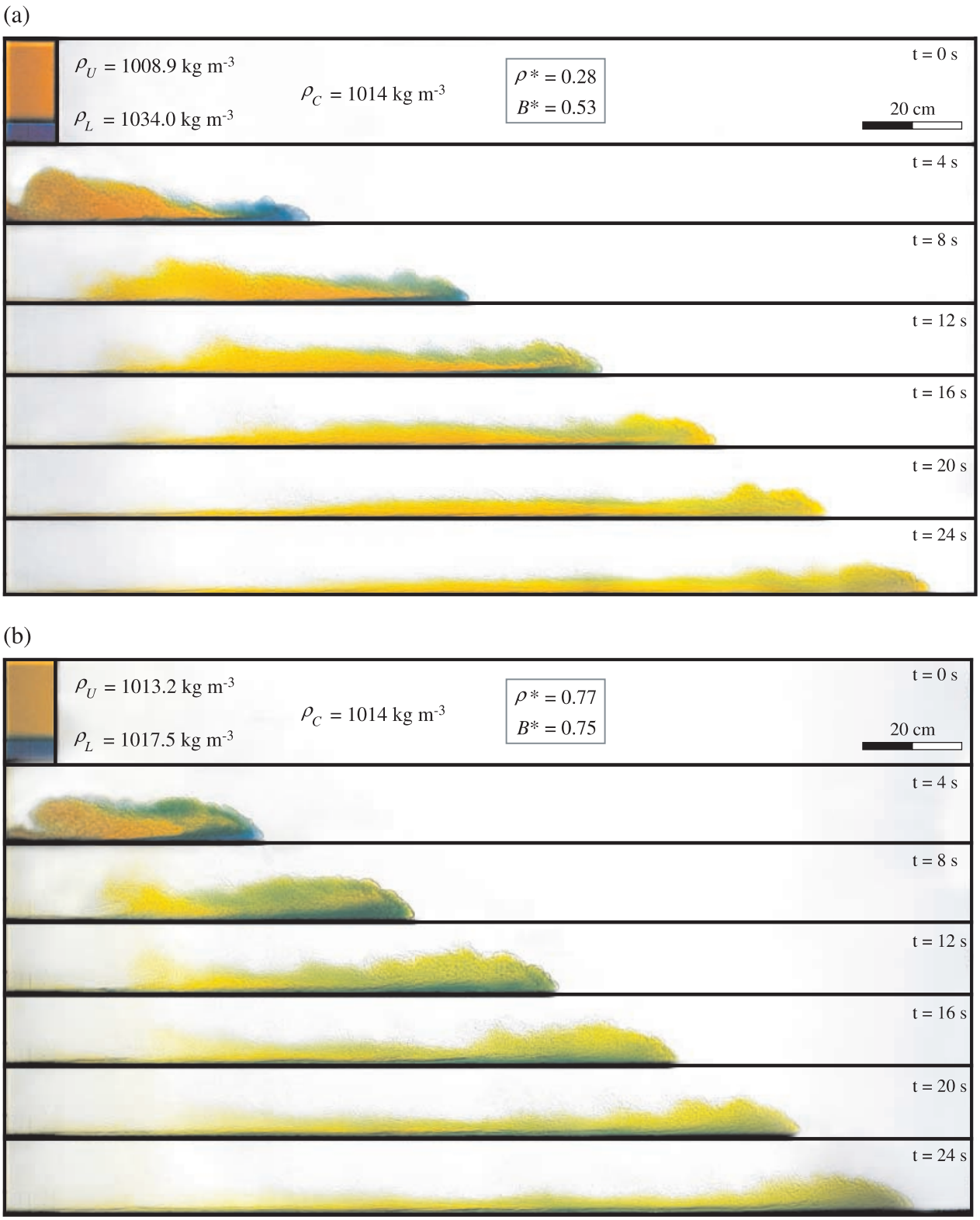

Fig. 7. Photographs of two-layered currents from series C ($B^* > 0{\cdot}5$) where the mass of salt in the lower layer, M_L, is less than that in the upper layer, M_U, so $\rho_U h_U > \rho_L h_L$ and the upper layer contains more of the driving buoyancy than the lower layer. In both flows, the upper layer travels to the flow front to drive the flow. (a) In the strongly stratified current (Expt C4), this occurs through overtaking, resulting in streamwise and vertical stratification. (b) In a weakly stratified current (Expt C1), this occurs through mixing of the layers.

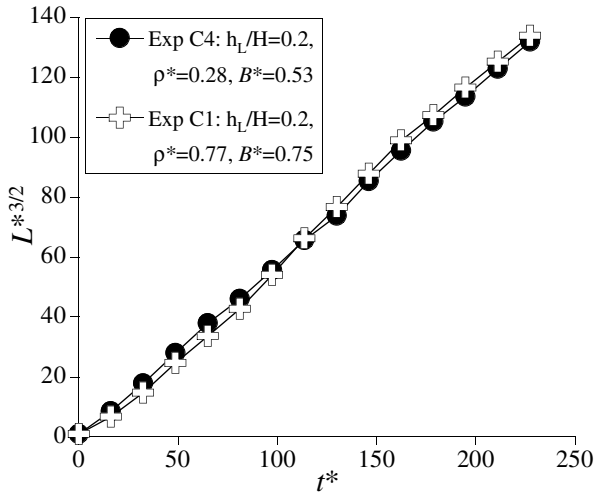

Fig. 8. Dimensionless distance–time data are plotted for the two flows photographed in Fig. 7, Expts C4 and C1, where the upper layer contains more driving buoyancy than the lower layer ($B^* > 0{\cdot}5$). The straight-line collapse confirms that, despite the thin lower layer in these experiments, both flows are described well by the inertial scalings given in Eqs (7) and (8), indicating that drag does not influence their behaviour over the duration of the experiment considered.

similar density, they mix rapidly as observed in series B, and the upper layer lags behind forming a thin, elongate wedge (Figs 5a and 9b). Lastly, when the driving buoyancy is fairly evenly distributed between the three layers, they mix rapidly during initial propagation. The middle layer intrudes into the lower layer as a wedge below the wake and they both mix (Fig. 9c), with the upper layer then intruding into this new mixed current and the whole current becoming thoroughly mixed. The scaled distance–time plots demonstrate that drag plays a part in the deceleration of the flow in experiments where the density contrast between the lower and upper layers is large (Fig. 10).

DISCUSSION

From the observations and measurements on a range of stratified inertial gravity currents, a regime diagram has been constructed describing the flow dynamics in terms of the initial vertical stratification (Fig. 11). This work has established that the evolving morphology depends on: (1) the initial density contrast between the layers; and (2) the distribution of the driving buoyancy, controlled in these experiments by varying layer depth. Two dimensionless parameters can be defined to capture these initial conditions. First, a density ratio, ρ^*, which is simply the density of the upper layer divided by the density of the lower layer, both relative to the density of the ambient fluid (Eq. 10). The second parameter describes the distribution of buoyancy between the layers, B^*, and depends on both the density and the volume (or depth) of each layer (Eq. 11). B^* is therefore proportional to the mass of salt present in each layer. The four types of flow evolution presented in Figs 5 and 7 can now be described in terms of ρ^* and B^* (Fig. 11).

For all flows, the layer with the highest driving buoyancy, i.e. that containing the greatest mass of salt, travels to the nose of the current and drives the flow. This is consistent with the simple relationship from Eq. (1) that $u \sim (B_0/L)^{1/2}$. When there is a large density contrast between the layers (small ρ^*), they do not mix significantly during this process, and streamwise flow stratification occurs. However, when the density contrast between the layers is small ($\rho^* \rightarrow 1$), pronounced mixing occurs leading to the development of a more homogeneous flow. The layer at the rear of the flow propagates forward along the density interface between the lower dense body region and the upper dilute turbulent wake region of the flow, reflecting its intermediate density.

Drag can be important when the lower layer is both thin and of high density compared with the upper layer. The lack of mixing and dilution causes the flow to remain thin and become retarded by friction. This is not the case if the lower layer is thin and of similar density to the upper layer: the mixing between the layers causes the current to thicken and overcome the effects of drag. Successful description of these flows by the inertial scalings in Eqs (7) and (8) indicates that, for many of these density-stratified flows, it is possible to neglect the influence of dissipation through friction and viscosity on the flows over the temporal and spatial range considered here.

The slumping of laboratory gravity currents

The visualization of dyed layers allows observation of the slumping mechanism of fixed-release laboratory gravity currents as they collapse downwards and out of the confines of a lock region and into the ambient surroundings upon removal of the lockgate. In all experiments, both flows that are weakly or strongly stratified (Figs 5, 7 and 9a and b) and nearly homogeneous (Fig. 9c) collapse in the same manner. Fluid slumps out of the lock

(a)

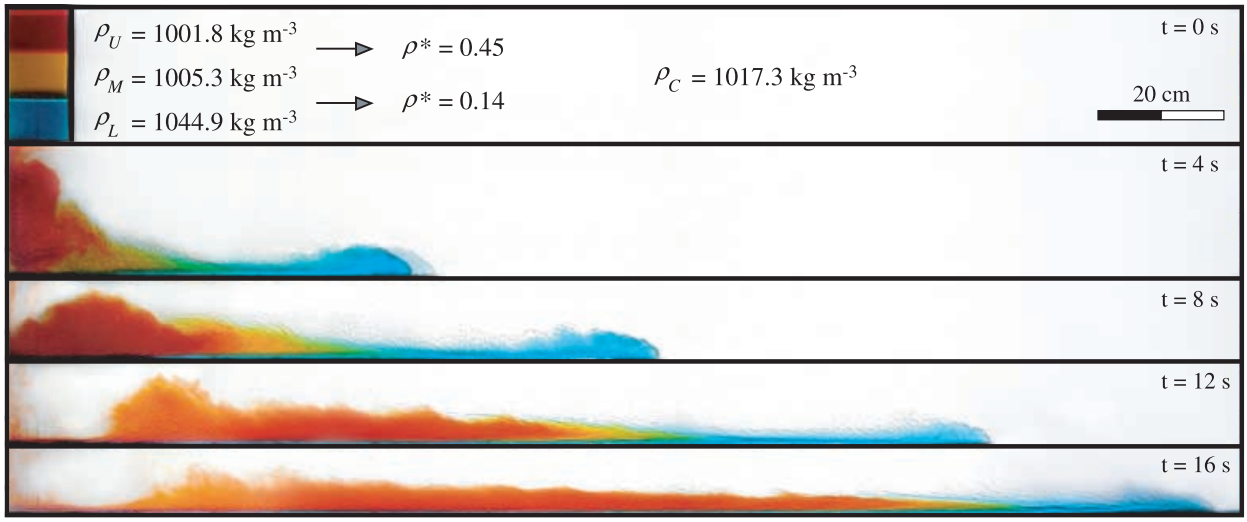
ρ_U = 1001.8 kg m^{-3}
ρ_M = 1005.3 kg m^{-3}
ρ_L = 1044.9 kg m^{-3}
ρ^* = 0.45
ρ^* = 0.14
ρ_C = 1017.3 kg m^{-3}
t = 0 s
20 cm
t = 4 s
t = 8 s
t = 12 s
t = 16 s

(b)

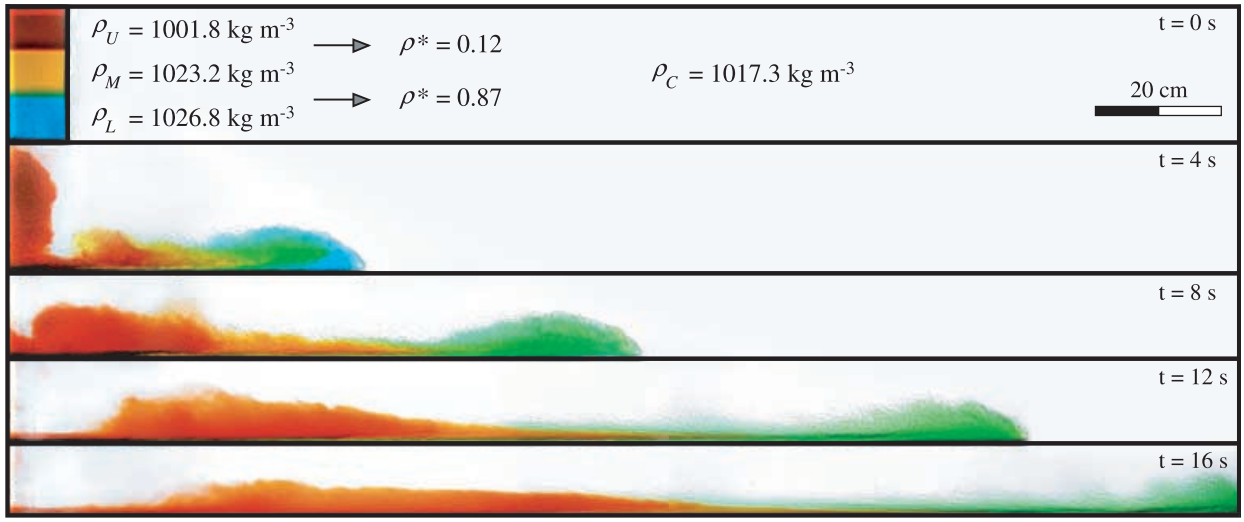
ρ_U = 1001.8 kg m^{-3}
ρ_M = 1023.2 kg m^{-3}
ρ_L = 1026.8 kg m^{-3}
ρ^* = 0.12
ρ^* = 0.87
ρ_C = 1017.3 kg m^{-3}
t = 0 s
20 cm
t = 4 s
t = 8 s
t = 12 s
t = 16 s

(c)

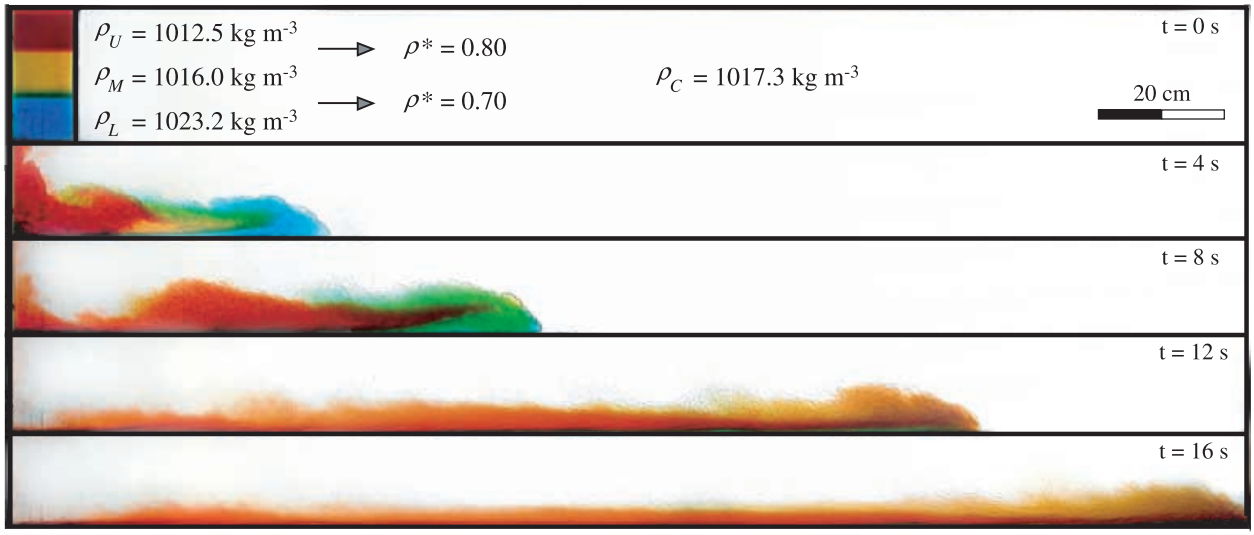
ρ_U = 1012.5 kg m^{-3}
ρ_M = 1016.0 kg m^{-3}
ρ_L = 1023.2 kg m^{-3}
ρ^* = 0.80
ρ^* = 0.70
ρ_C = 1017.3 kg m^{-3}
t = 0 s
20 cm
t = 4 s
t = 8 s
t = 12 s
t = 16 s

Fig. 9. Photographs of three-layered saline currents from series D: these flows have three layers of equal depth and the same total current density $\rho_C = 1017{\cdot}3$ kg m^{-3}, but the distribution of this density between the layers is varied (Table 1). (a) The lower layer has the greatest density and buoyancy (Expt D1). (b) The lower two layers have a small density contrast between them but a large density contrast with the upper layer (Expt D2). (c) The driving buoyancy is more evenly distributed throughout all three layers, approximating a homogeneous flow (Expt D3).

region sequentially, with fluid initially at the base of the lock leaving first to form the front of the flow, and fluid initially at the top of the lock leaving last to form the rear of the flow. The sequence of photographs presented here illustrates how fluid towards the centre and rear of the flow propagates forward by forming a wedge-shaped intrusion into the back of the head along a density interface. This interface separates the more concentrated body of the flow from the dilute turbulent wake region that develops through shedding of fluid immediately behind the flow head. The nature of this intrusion is particularly clear in the multiple-layered currents (Fig. 9), and the new observations provide important information on the initial propagation of lock-exchange laboratory flows.

Scaling of laboratory flows

Two dimensionless numbers can be used to characterize the dynamics of these inertial experimental flows. Consideration of these numbers indicates that the experimental models of turbidity currents and pyroclastic density currents are dynamically similar to their natural counterparts as (1) the Reynolds number, *Re*, of both the experimental and natural flows is sufficiently large to be turbulent, at least during the early stages of the experimental flows, and (2) the Froude number at the head of the current, *Fr*, is of order unity, a value that is thought to apply to the natural counterparts (Simpson, 1997).

The Reynolds number is evaluated here using

$$Re = \frac{uh_C\rho}{\mu} \qquad (12)$$

where u is the velocity of the front of the flow, h_C the thickness of the current, and ρ and μ are the density and viscosity of the fluid driving the flow respectively. Using the photographs in

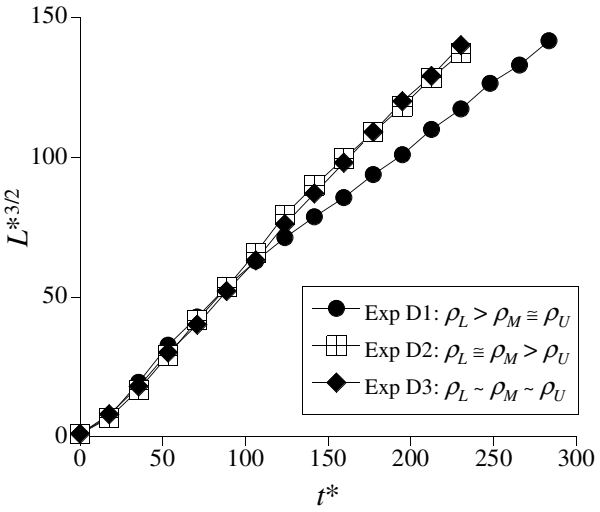

Fig. 10. Distance–time data for the three-layer currents are scaled as before using Eqs (7) and (8). The deviation of flow D1 indicates that this flow is no longer purely inertial. This flow was driven by an extremely dense lower layer containing most of the buoyancy, compared with the overlying middle and upper layers. This causes the lower layer to run ahead of the remaining flow, where it thins and becomes affected by drag.

Figs 5 and 7, u and h can be estimated at time steps of 4 s, although there are significant errors associated with h because it is difficult to define the upper boundary of the current. In those experiments in which the two layers mix (B26 and C1), ρ and μ are taken as the average of the two layers. In the experiments in which one layer leads the flow, the initial density and viscosity of this layer is used in the *Re* calculation.

Figure 12a shows the change in *Re* for each of the four photographed flows (Figs 5a and b, 7a and b). The overall trend is for *Re* to decrease with time from around 7500 to 3000, reflecting the decrease in velocity during propagation. At longer times and distances, beyond the range of the photographs, *Re* for some flows decreases to $\approx$1000, but the *Re* is mostly above the critical value for the transition to turbulence, which has a value of the order 2000 for turbulent gravity currents (Simpson & Britter, 1979; Allen, 1985). Therefore, the laboratory flows are considered to be reasonable analogues for natural gravity currents with much greater Reynolds numbers. However, the results of the experiments are probably best applied to those flows that are waning and depositional, not erosional. The experimental flows that become strongly influenced by friction at the base have been clearly

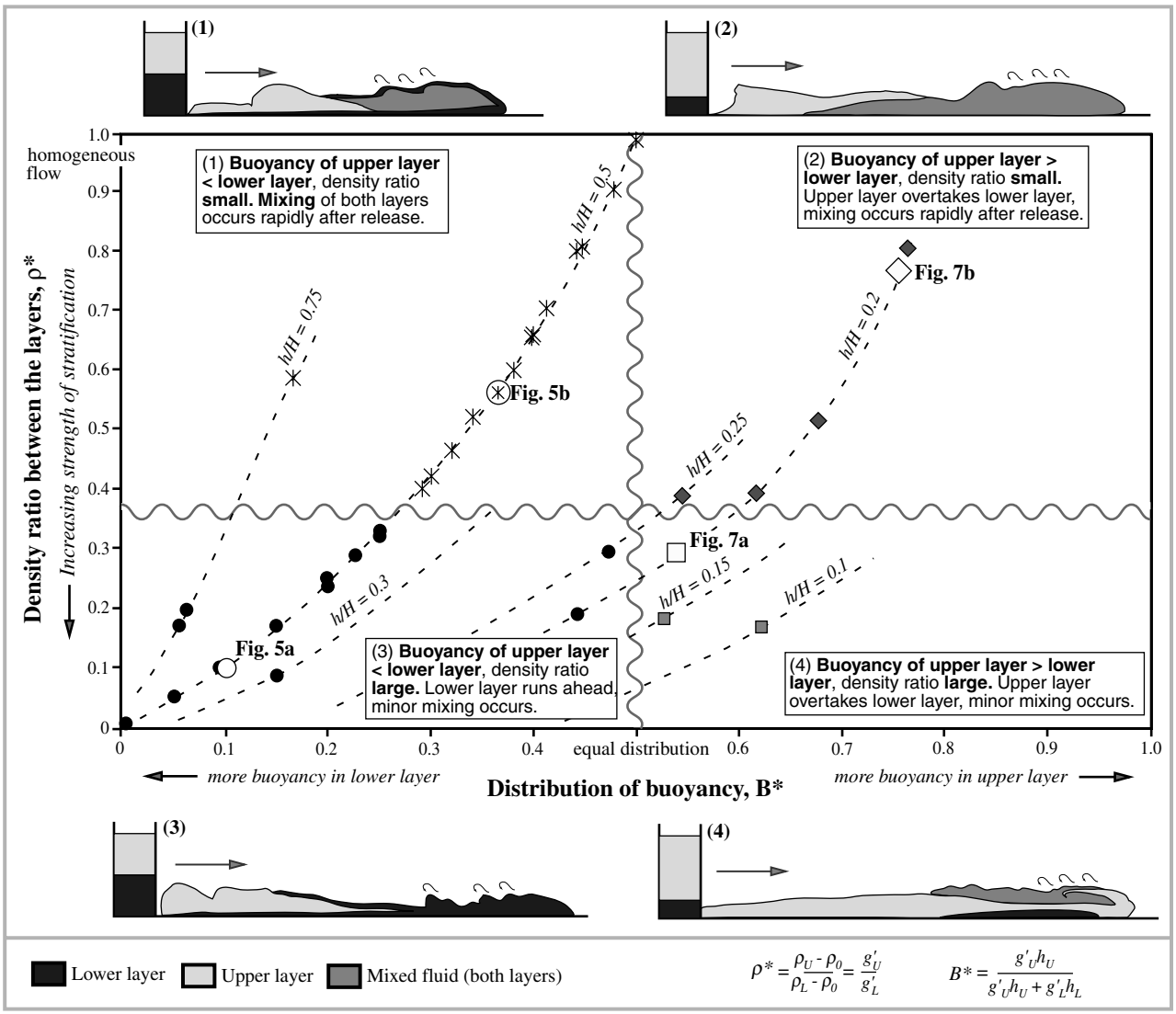

Fig. 11. A regime diagram can be constructed from the experimental observations, summarizing the flow behaviours of two-layer density-stratified inertial currents, in terms of a dimensionless density ratio ρ^* (y-axis) and dimensionless distribution of buoyancy between the layers, B^* (x-axis). Schematic cartoons of the flow behaviour are shown for each quadrant. The figure numbers marked at specific data points cross-refer to photographs of each flow behaviour.

identified through the scaled distance–time plots.

A second consideration is the densiometric Froude number, *Fr*, calculated at each 4 s time interval for the four photographed experiments (Figs 5 and 7) using

$$Fr = \frac{uL^{1/2}}{B_0^{1/2}} \qquad (13)$$

Figure 12b validates the application of a constant Froude number scaling in these experiments. Although there is some scatter during the initial slumping part of the flow, *Fr* levels off to $\approx 1{\cdot}3$. This is of order unity, in accordance with natural full-scale turbulent flows.

Analysis of regimes

The experimental results indicate that there are two key processes occurring during the propagation of two-layer, density-stratified inertial flows: (1) streamwise stratification of the flow resulting from separation of the layers, owing to their different flow velocities; and (2) mixing of the two layers promoting the development of a homogeneous current. The buoyancy contrast, B^*, controls the degree of separation, while the mixing of

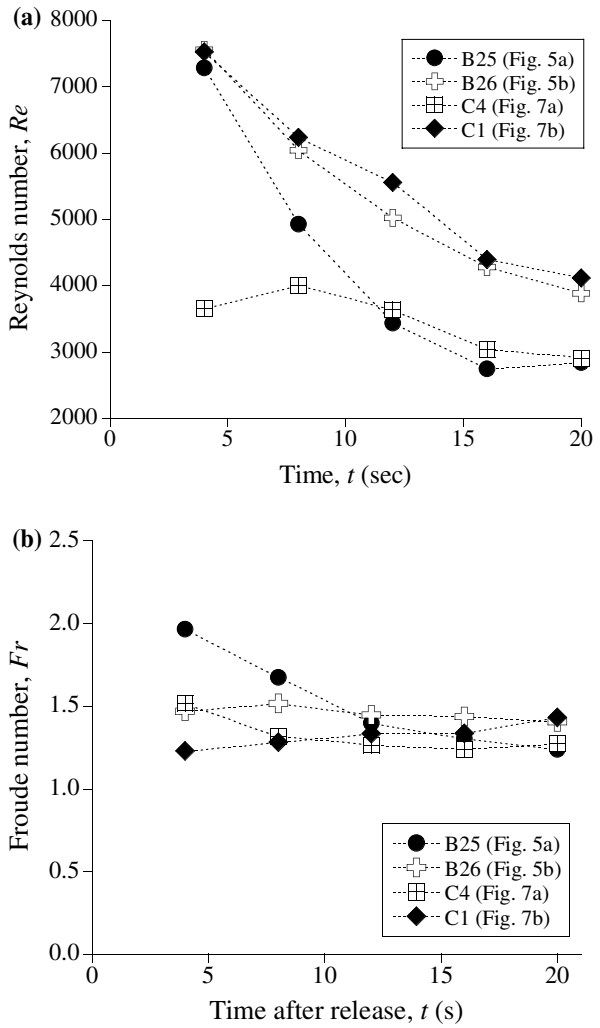

Fig. 12. (a) The Reynolds number, *Re*, is calculated using Eq. (12) for each of the four photographed flows. *Re* declines from around 7000 to 3000 during propagation, suggesting that, although they are turbulent, these laboratory flows are probably best applied to waning, depositional turbidity currents. (b) The Froude number, *Fr*, is calculated using the nose conditions of Eq. (13) for the four flows (B25, B26, C4 and C1). Although there is a degree of initial scatter, the Froude number is approximately constant at $Fr = 1{\cdot}3$.

the layers is a function of their density contrast, ρ^*. To understand these competing processes, a timescale for each is derived. Observations suggest that the process that dominates during the initial stages of an experiment controls the subsequent evolution of the experimental flow, i.e. once streamwise stratified, the flow is unable to mix and, conversely, once mixed, it is unable to stratify in the streamwise direction. Therefore, consideration of these processes in the early stages provides information on the development of the flow throughout an experiment. The timescale over which the layers separate by a distance L_0 is compared with the timescale over which the layers mix vertically across the full current depth, h_C. Note that these scalings are simple functional forms and do not include numerical factors.

If the two layers comprising the initial vertical stratification are considered as separate flows propagating forwards after gate release (Fig. 13), then the time taken for them to separate by a distance L_0 will depend on the velocity difference between the layers:

$$\tau_{SEP} \sim \frac{L_0}{(u_L - u_U)} \tag{14}$$

where u_L and u_U are the speeds of the lower and upper layers respectively.

A timescale describing the development of a mixed zone, τ_{MIX}, between the two layers to the full depth of the flow, h_C, can be defined (Fig. 13):

$$\tau_{MIX} \sim \frac{h_C}{(\mathrm{d}h_{MIX}/\mathrm{d}t)} \tag{15}$$

where the rate of growth, $\mathrm{d}h_{MIX}/\mathrm{d}t$, depends on a characteristic velocity for mixing, $\hat{u}$, and an entrainment coefficient, ϵ, which describes the mixing by eddies at the interface between the two layers and is a function of the Richardson number, *Ri* (e.g. Strang & Fernando, 2001). Although it is difficult to estimate *Ri* at the mixing interface, it is possible to measure the bulk Richardson number for these stratified flows because $Ri_B = 1/Fr$. The Froude number for the present experiments is $\approx 1{\cdot}2$–$1{\cdot}5$ (Fig. 12b) giving $Ri_B = 0{\cdot}6$–$0{\cdot}8$. At these values of *Ri*, an inverse entrainment law, $\epsilon = \alpha/Ri$, is a reasonable approximate parameterization, where α is an entrainment constant (Turner, 1979). This leads to the relation

$$\frac{\mathrm{d}h_{MIX}}{\mathrm{d}t} \sim \hat{u}\left(\frac{\alpha}{Ri}\right) \tag{16}$$

where *Ri* is

$$Ri = \frac{(g'_L - g'_U)h_C}{\hat{u}^2} \tag{17}$$

leading to the scaling

$$\tau_{MIX} \sim \frac{(g'_L - g'_U)h_C^2}{\alpha\hat{u}^3} \tag{18}$$

and h_C is evaluated here as the total initial depth of the current. Note that there are many

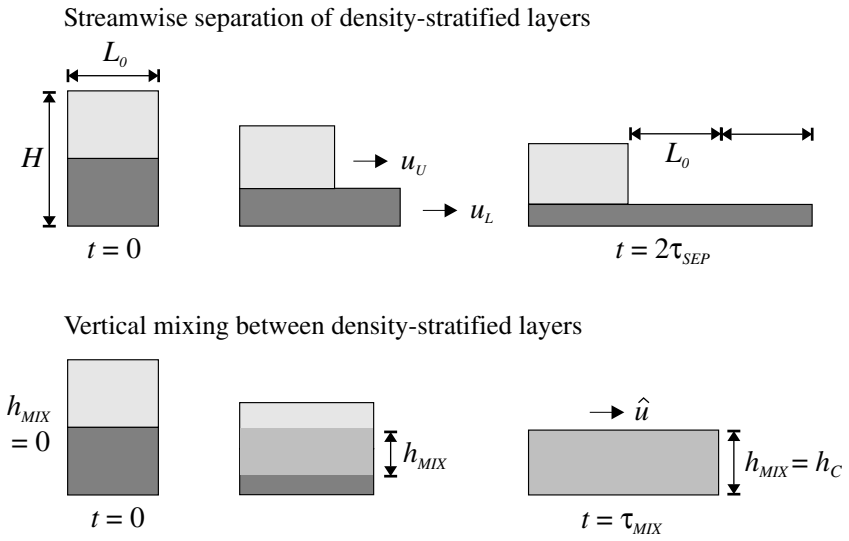

Fig. 13. Sketches showing the separation of two layers by a distance L_0 over a timescale τ_{SEP} owing to their buoyancy difference, and the vertical mixing of the two layers to a depth h_C over a timescale τ_{MIX} owing to their density contrast. The relative importance of these two processes during the early part of an experiment controls the overall development of the flow morphology.

alternative models describing the entrainment and subsequent mixing, and each may lead to a different functional form for τ_{MIX} (e.g. Parsons & Garcia, 1988; Caulfield & Kerswell, 2001) The characteristic velocity for mixing, $\hat{u}$, will depend on the layer propagating with the fastest velocity. The experiments have indicated that the layer with the higher buoyancy, and thus faster velocity, drives the flow, and so $\hat{u}$ is approximated by:

$$\hat{u} \approx \frac{B_0^{1/2}}{L_0^{1/2}} \tag{19}$$

The transition between layers that mix and layers that separate in a streamwise or longitudinal direction is given by the condition

$$\tau_{SEP} = \tau_{MIX} \tag{20}$$

and, using Eqs (18) and (14), this occurs when

$$\frac{\tau_{MIX}}{\tau_{SEP}} \sim k\left(\frac{\sqrt{\hat{B}}}{\sqrt{B_L} - \sqrt{B_U}}\right)\left(\frac{\hat{g}'}{g'_L - g'_U}\right) = 1 \tag{21}$$

Here, $\hat{g}'$ and $\hat{B}$ are the reduced gravity and buoyancy, respectively, of fluid travelling with velocity $\hat{u}$ and $k = \alpha L_0/H$. The transition curve depends on the buoyancy difference $\hat{B}^{1/2}/(B_L^{1/2} - B_U^{1/2})$ or velocity difference $\hat{u}/(u_L\text{-}u_U)$, and the reduced gravity difference between the layers $\hat{g}/(g_L - g_U)$. This agrees qualitatively with the experimental observations that the behaviour of the flow depends on the buoyancy distribution, B^* (on which velocity depends) and the density ratio, ρ^*. All the experiments from Fig. 11 are now presented in terms of the initial dimensionless buoyancy difference and initial dimensionless reduced gravity difference between the layers (Fig. 14). The transition curve of Eq. (21) has been added. Note that a different curve will result if an alternative dependency of α on Ri is used, and that this curve is simply a functional form rather than a full model. Nevertheless, it is in good accordance with the experimental observations: the scalings indicate four possible regions of behaviour, and most of the experimental data are consistent with the analysis, with a small

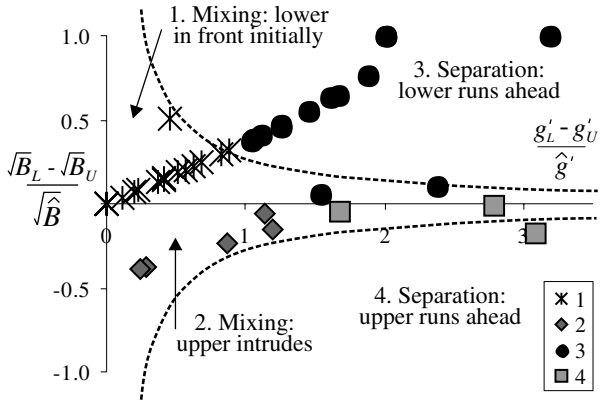

Fig. 14. The experimental data points from Fig. 11 are plotted with the scaling law of Eq. (21), which describes the transition between mixing of the two layers and separation of the layers in the initial stages of the flow. This validates the experimental observation that the initial buoyancy contrast, on which velocity differences scale, and the initial density or reduced gravity contrast can be used to understand the evolution of laboratory density-stratified flows.

scatter in the immediate vicinity of the transition curve itself. This validates the interpretation of the experimental results that the development of these laboratory flows depends on the balance between mixing and separation processes during early parts of an experiment, and this can be captured by a simple scaling relation based on the initial conditions.

IMPLICATIONS FOR NATURAL CURRENTS AND THEIR DEPOSITS

The effects of grain size and concentration stratification in the flow will influence the characteristics of their deposits and, in particular, lateral, streamwise and vertical characteristics may be accentuated. Consider a strongly stratified flow, either sedimentary or volcanic, with gradients in both concentration and grain size, where the dense lower part of the flow surges ahead of the upper parts of the current. However, this lower part of the flow would also deposit more rapidly because the coarse-grained components are close to the base of the flow. This would be expected to produce a more pronounced lateral segregation of particles and facies variations, with coarse particles being deposited rapidly from the base of the flow. If deposition is considered at a fixed spatial point, then the lateral structure of the flow will lead to more pronounced vertical changes in sediment, grain size and sedimentary structures.

In particle-laden flows, a complex evolution of the flow may occur as the lower layer deposits particles and loses buoyancy. If the lower layer carries the larger grains, then the buoyancy of the lower layer may decrease towards that of the upper layer, leading to a transition from a well-stratified flow to a more well-mixed flow as the current moves downstream. This may, over time, lead to a transition between layered deposits near source and well-mixed deposits further from source. In currents where the upper layer has greater buoyancy than the lower layer, then the upper part would be expected to overtake the nose, and well-mixed or even reverse-graded deposits would be formed further downstream. In a strongly stratified natural current, the coarse-grained lower part of the current may initially surge ahead and detach from the dilute upper part leading to two discrete deposits. Particle-laden currents formed by a weakly stratified initial mixture would possibly produce deposits of a homogeneous nature, as thorough mixing would occur in the early stages of propagation.

Application to pyroclastic density currents (PDCs)

In volcanic flows, there are a number of studies in which the deposits can be closely linked to observed flows. The volcanic blast of 26 December (Boxing Day) 1997 at the Soufrière Hills volcano, Montserrat, provides an opportunity to consider the extent to which stratification is an important attribute. This event was initiated by major collapse of a volcanic edifice and the lava dome within, generating a highly energetic directed PDC (Sparks *et al.*, 2002). The PDC formed deposits that exhibit significant lateral and vertical lithofacies variations in terms of grain size, thickness and the development of bedforms. The deposits are characterized by a lower coarse-grained, normally graded layer (layer 1) overlain by a finer grained, well-stratified upper layer (layer 2) (Gladstone & Sparks, 2002; Ritchie *et al.*, 2002). The transition between layers 1 and 2 is typically well-defined and abrupt, suggesting deposition from a flow that is stratified in both vertical and streamwise directions. Deposition from a stratified PDC in which the lower dense layer supporting and depositing coarse grains had surged ahead during the early stages, with subsequent deposition from a finer region of the flow that had lagged behind, could account for these features (cf. Fig. 5a). In addition, substantial changes in the median grain size of layer 1 were observed to occur where the current moved obliquely across deep valleys in the flank of the volcano, suggesting that the coarser grained and denser lower parts of the current were diverted into the valleys while the upper fine-grained parts were less affected by this topography. The field observations at Montserrat suggest that the 26 December PDC was both vertically stratified, causing confinement of the dense, coarse parts of the flow to valleys, and stratified in a streamwise direction, leading to the formation of a grain-size break in the deposit.

The effects of stratification observed in the experimental series may also explain the transition from a well-sorted, layered deposit near the vent to a more homogeneous deposit far afield as displayed in PDC deposits generated at Bezymianny volcano, Kamchatka Peninsula, Russia, in 1956 (Belousov, 1996). It is envisaged that initially the dense lower layer of the PDC current runs ahead and, as the lower layer deposits coarse particles, the buoyancy difference between the layers will decrease. Eventually, the upper layer can catch up

with, and mix with or over-run, the initially dense basal parts of the flow (Figs 5a and 7a).

Application to turbidity currents

In common with the features of PDC deposits, the deposits of turbulent subaqueous flows, turbidites, also show marked lateral and vertical facies variations. The new insights on density-stratified flows from the present experiments are applied to understand certain features of these deposits, building on previous experimental studies that provide information on the development of internal stratification and the implications for resulting facies (e.g. Postma *et al.*, 1988; Kneller *et al.*, 1999).

Vertical grain-size characteristics of turbidites can provide important information on the lateral and streamwise features of the depositing flow; for example, sharp discontinuities separating a single bed into zones or layers characterized by different grain sizes are well documented in the rock record. Features such as these are often attributed to self-stratification of particles within the flow (McCave & Jones, 1988; Choux & Druitt, 2002; Gladstone & Sparks, 2002). Flow reflection and the interaction with topography may also contribute to stratification in specific cases (Pickering & Hiscott, 1985; Kneller *et al.*, 1991; Edwards *et al.*, 1994). In particular, stratification is expected to develop during ambient entrainment and sediment erosion by currents feeding down through submarine canyons. When these currents exit on to the low slopes of a basin floor and transform from erosional or non-depositional to depositional, it is likely that they are already strongly stratified in grain size and sediment concentration. In these circumstances, the effects identified in the present paper resulting from concentration stratification will influence the dispersal and characteristics of the resulting deposits.

The new experiments illustrate that, under certain conditions (Fig. 11), vertical stratification leads to streamwise stratification. In the case in which there is a strong initial vertical stratification and the lower layer contains most of the driving buoyancy, the experiments show that the lower layer will form the leading part of the gravity current, whereas the upper part of the vertical stratification forms the rear part of the current. In a particulate flow, coarser grains will settle towards the base of the vertical stratification while finer grains will remain within the upper layer and so, during development of the streamwise stratification, the coarse particles will be transported within the leading part of the current and the fine grains towards the rear of the current (cf. Fig. 5a). Assuming this flow deposits along its length, the resulting bed will be normally graded, comprising a lower region containing coarse grains deposited from the front of the flow overlain by the finer grains deposited from the rear of the flow. If the initial density ratio between the layers was large, and so mixing between the layers suppressed, the change between the basal coarse part of the bed and the overlying fine part would be sharp, causing a grain-size break. If the initial density ratio was smaller, some mixing would occur between the layers leading to a deposit characterized by more gradual upward fining.

The above example is based on the notion that the concentrated lower layer, dyed blue in the experiments, is a proxy for the initially denser and coarser part of the flow, while the upper layer, dyed yellow, is a proxy for the less concentrated region of the flow that supports and deposits the finer grains. The laboratory photographs show that the interaction between these layers during flow propagation is not straightforward: the rear region of the flow moves forward by intruding along the concentration interface between the body and wake regions of the flow. While this leads to a flow that has a consistent density or concentration profile (i.e. the densest part of the flow remains at the base and the least dense part at the top), the vertical grain-size profile will be variable, with a finer grained region located between two coarser grained regions (e.g. Fig. 5b). It is difficult to infer the grain-size characteristics of a bed deposited by such a flow; one possibility would be an upward-fining deposit with an anomalously coarse horizon towards the top of the bed. Nevertheless, extrapolating the observations from individual experiments to turbidity currents suggests that a range of bed characteristics can be produced by small variations in the volume and concentration of the layers forming the initial vertical profile of the flow.

Finally, the same effects of topography inferred for pyroclastic density currents can be anticipated when turbidity currents that are already stratified exit canyons and spread over the proximal parts of a submarine fan. The denser and coarser grained lower region of the current can be expected to be more influenced by fan topography and to be captured by fan channels, whereas the upper more dilute and finer grained region of the

current will be unconstrained and can expand over a wider region. Exactly where different facies will be distributed will depend on the extent of the initial stratification. A strongly stratified current can be expected to show a much more marked lateral and topographically related facies variation than a homogeneous or weakly stratified current with the same sediment mix.

CONCLUSIONS

The dynamics of inertial gravity currents that are initially stratified in density have been examined through systematic laboratory experiments. These experiments have identified that the initial vertical stratification may lead to significant streamwise stratification of the flow if the density ratio between the layers is sufficiently large. Moreover, the experiments have identified that the layer containing the greatest buoyancy will propagate to the nose of the flow and drive the current. This may, in some circumstances, be the upper, less dense layer. The experiments also show that the layers propagate forward by intruding along a density interface between the body and wake regions of the current. The degree of mixing between the two layers during this process depends on the initial density ratio, i.e. the strength of the stratification, between the layers. The intrusion of fluid in such stratified flows leads to a more complicated vertical profile than that initially imposed on the flow.

By balancing two simple scalings, the competition is described between the early separation of the layers owing to their velocity differences and the vertical mixing at the interface between the layers. The scaling law for the regime transition agrees reasonably well with the range of observations on the evolution of two-layer density-stratified currents, validating the interpretation from the experiments that the buoyancy contrast controls separation while the density contrast controls mixing. The role of sedimentation on this transition, in particular the case in which the time over which sedimentation occurs becomes comparable to the shorter of either the mixing or the separation times presented here, forms a fruitful area for future research.

The gradual sedimentation of grains from particulate flows stratified vertically and/or in the streamwise direction may account for the wide range of grading characteristics commonly found in the deposits of turbidity and pyroclastic density currents. For example, if a coarse-grained, denser, lower layer and fine-grained, less-dense, upper layer stratify in a streamwise direction, a normally graded deposit with a grain-size break will result. However, if the density ratio between the layers is small, a more gradual upward-fining deposit may characterize the deposit. The intrusion of a rear layer containing fines into a coarse-grained flow at the body–wake interface could be a mechanism for transporting coarse particles to high levels within the flow; as the flow wanes, these might sediment out as anomalously coarse horizons in a predominantly fine-grained zone of the bed. Finally, stratified natural flows will be affected by topography: a lower dense region may be captured within canyons while an upper dilute region can expand over a wide area. The extent of this interaction will be a function of the stratification, and therefore grain size and concentration stratification will affect not only the internal details of individual beds, but also the development and architecture of turbidite fans.

ACKNOWLEDGEMENTS

C.G. thanks the Isaac Newton Trust and BP Institute for funding, L.J.R. the University of Luton and BP Institute, and R.S.J.S. a NERC Fellowship and Royal Society Wolfson Award. The authors would like to thank Jeff Parsons for a thorough review and discussion, and an anonymous reviewer for useful comments that improved the manuscript substantially. Also, many thanks to Jim Best for his detailed input and suggestions, Mats Nigam for fruitful discussion, and Dudley Simons for photographic assistance.

NOTATION

A, A_0 area of the gravity current (i.e. two-dimensional volume); initial current area

α entrainment constant characterizing the vertical mixing between the layers

B, B_0, B_U, B_L buoyancy of the flow ($= g'A$), initial total buoyancy, upper layer buoyancy and lower layer buoyancy respectively

$\hat{B}$ buoyancy of fluid which travels with velocity $\hat{u}$ and characterizes the vertical mixing between the layers

B^* dimensionless buoyancy distribution between the layers $= M_U/(M_U + M_L)$, Eq. (11)

ϵ an entrainment coefficient $= \alpha/Ri$

Fr Froude number, Eq. (13)
g gravitational acceleration
g', g'_0, g'_U, g'_L reduced gravity of the whole flow, whole flow initially, upper layer only and lower layer only respectively
$\hat{g}'$ reduced gravity of fluid that travels with velocity $\hat{u}$ and characterizes the vertical mixing between the layers
h_C, h_U, h_L, h_M depth of current, upper layer, lower layer and middle layer (three-layer experiments only) respectively
h_{MIX} vertical depth of the mixed zone that develops between the two layers
H total depth of lock, which equals depth of ambient
L, L_0 length of current and lock length
L^* dimensionless current length, Eq. (7)
M_U, M_L mass of salt in the upper layer, proportional to $\rho_U h_U$, and lower layer ($\rho_L h_L$) respectively
μ kinematic fluid viscosity
t time
t^* dimensionless time, Eq. (8)
τ_{SEP}, τ_{MIX} timescales describing the early separation of, or vertical mixing between, the upper and lower layers respectively, Eqs (14) and (18)
Re Reynolds number, Eq. (12)
Ri Richardson number, Eq. (17)
ρ_0, ρ_U, ρ_L, ρ_C density of the ambient fluid, upper layer, lower layer and whole current respectively
ρ^* dimensionless density ratio between the layers $= g'_U/g'_L$, Eq. (10)
u, u_L, u_U velocity of the flow front, upper layer only and lower layer only respectively
$\hat{u}$ characteristic velocity for vertical mixing between the two layers, Eq. (19)

REFERENCES

Allen, J.R. (1985) *Principles of Physical Sedimentology*. George Allen & Unwin, London, 272 pp.

Belousov, A. (1996) Deposits of the 30 March 1956 directed blast at Bezymianny Volcano, Kamchatka, Russia. *Bull. Volcanol.*, **57,** 649–662.

Benjamin, T.B. (1968) Gravity currents and related phenomena. *J. Fluid Mech.*, **31,** 209–248.

Bonnecaze, R.T., Huppert, H.E. and **Lister, J.R.** (1993) Particle driven gravity currents. *J. Fluid Mech.*, **250,** 339–369.

Buckee, C.M., Kneller, B.C. and **Peakall, J.** (2001) Turbulence structure in steady, solute-driven gravity currents. In: *Particulate Gravity Currents.* (Eds J. Peakall, W.D. McCaffrey and B.C. Kneller), *Int. Assoc. Sedimentol. Spec. Publ.*, **31,** 173–188.

Caulfield, C.P. and **Kerswell, R.R.** (2001) Maximal mixing rate in turbulent stratified Couette flow. *Phys. Fluids*, **13,** 894–900.

Choux, C.M. and **Druitt, T.H.** (2002) Analogue study of particle segregation in pyroclastic density currents, with implications for the emplacement mechanisms of large ignimbrites. *Sedimentology*, **49,** 907–928.

Clayton, C.J. (1994) Contrasting sediment gravity flow processes in the late Llandovery, Rhuddnant Grits turbidite system, Welsh Basin. *J. Geol.*, **29,** 167–181.

Dade, W.B. and **Huppert, H.E.** (1995) Axisymmetric particle-driven gravity currents. *J. Fluid Mech.*, **294,** 93–121.

Druitt, T.H. (1998) Pyroclastic density currents. In: *The Physics of Explosive Volcanic Eruptions* (Eds J.S. Gilbert and R.S.J. Sparks), *Geol. Soc. London Spec. Publ.*, **145,** 145–182.

Edwards, D.A., Leeder, M.R., Best, J.L. and **Pantin, H.M.** (1994) On experimental reflected density currents and the interpretation of certain turbidites. *Sedimentology*, **41,** 437–461.

Gladstone, C. and **Sparks, R.S.J.** (2002) The significance of grainsize breaks in turbidites and pyroclastic density current deposits. *J. Sed. Res.*, **72,** 182–196.

Gladstone, C. and **Woods, A.W.** (2000) A note on the application of box-models to particle-driven gravity currents. *J. Fluid Mech.*, **416,** 187–195.

Hallworth, M.A., Huppert, H.E., Phillips, J.C. and **Sparks, R.S.J.** (1996) Entrainment in turbulent gravity currents. *Nature*, **362,** 829–831.

Hogg, A.J. and **Woods, A.W.** (2001) The transition from inertia- to bottom-drag-dominated motion of turbulent gravity currents. *J. Fluid Mech.*, **449,** 201–224.

Hopfinger, E.J. (1983) Snow avalanche motion and related phenomena. *Annu. Rev. Fluid Mech.*, **15,** 47–76.

Huppert, H.E. and **Simpson, J.E.** (1980) The slumping of gravity currents. *J. Fluid Mech.*, **99,** 785–799.

von Karman, T. (1940) The engineer grapples with non-linear problems. *Bull. Am. Math. Soc.*, **46,** 615.

Keulegan, G.H. (1957) An experimental study of the motion of saline water from locks into fresh water channels. *US Nat. Bur. Stan. Rep.*, **5168**.

Kneller, B.C. and **Buckee, C.** (2000) The structure and fluid mechanics of turbidity currents: a review of some recent studies and their geological implications. *Sedimentology*, **41,** 62–94.

Kneller, B.C. and **McCaffrey, W.D.** (1999) Depositional effects of flow nonuniformity and stratification within turbidity currents approaching a bounding slope: deflection, reflection, and facies variation. *J. Sed. Res.*, **69,** 980–991.

Kneller, B.C., Edwards, D., McCaffrey, W.D. and **Moore, R.** (1991) Oblique reflection of turbidity currents. *Geology*, **14,** 250–252.

Kneller, B.C., Bennett, S.J. and **McCaffrey, W.D.** (1999) Velocity structure, turbulence and fluid stresses in experimental gravity currents. *J. Geophys. Res.*, **104,** 5381–5391.

McCave, I.N. and **Jones, K.P.N.** (1988) Deposition of ungraded muds from high density non-turbulent turbidity currents. *Nature*, **333,** 250–252.

Middleton, G.V. (1966) Experiments on density and turbidity currents I. Motion of the head. *Can. J. Earth Sci.*, **3,** 523–546.

Middleton, G.V. (1993) Sediment deposition from turbidity currents. *Annu. Rev. Fluid Mech.*, **21,** 89–114.

Mulder, T. and **Alexander, J.** (2001) The physical character of subaqueous sedimentary density flows and their deposits. *Sedimentology*, **48,** 269–299.

Parsons, J.D. and **Garcia, M.H.** (1988) Similarity of gravity current fronts. *Phys. Fluids*, **10,** 3209–3213.

Pickering, K.T. and **Hiscott, R.N.** (1985) Continental (reflected) turbidity currents from the Middle Ordovician Cloridorme

Formation, Quebec, Canada: an alternative to the antidune hypothesis. *Sedimentology*, **32,** 373–394.

Postma, G., Nemec, W. and **Kleinspehn, K.** (1988) Large floating clasts in turbidites: a mechanism for their emplacement. *Sed. Geol.*, **58,** 47–61.

Ritchie, L.J., Cole, P.D. and **Sparks, R.S.J.** (2002) Sedimentology of deposits from the pyroclastic density current of 26th December 1997 at Soufrière Hills Volcano, Montserrat. In: *The Eruption of the Soufrière Hills Volcano, Montserrat, from 1995 to 1999* (Eds T.H. Druitt and B.P. Kokelaar), *Geol. Soc. London Mem.*, **21,** 435–456.

Schmidt, W. (1911) Zur Mechanik der Boen. *Z. Meterol.*, **28,** 355–362.

Simpson, J.E. (1997) *Gravity Currents in the Environment and the Laboratory*, 2nd edn. Cambridge University Press, Cambridge, 244 pp.

Simpson, J.E. and **Britter, R.E.** (1979) The dynamics of the head of a gravity current advancing over a horizontal surface. *J. Fluid Mech.*, **94,** 477–495.

Sinclair, H.D. (1994) The influence of lateral basinal slopes on turbidite sedimentation in the Annot Sandstones of SE France. *J. Sed. Res.*, **64,** 42–54.

Sparks, R.S.J., Barclay, J., Calder, E.S., Herd, R.A., Komorowski, J.C., Luckett, R., Norton, G.E., Ritchie, L.J., Voight, B. and **Woods, A.W.** (2002) Generation of a debris avalanche and violent pyroclastic density current on 26 December (Boxing Day) 1997 at Soufrière Hills Volcano, Montserrat. In: *The Eruption of Soufrière Hills Volcano, Montserrat, from 1995 to 1999* (Eds T.H. Druitt and B.P. Kokelaar), *Geol. Soc. London Mem.*, **21,** 409–434.

Stix, J. (2001) Flow evolution of experimental gravity currents: implications for pyroclastic flows at volcanoes. *J. Geol.*, **109,** 381–398.

Strang, E.J. and **Fernando, H.J.S.** (2001) Vertical mixing and transports through a stratified shear layer. *J. Phys. Oceanogr.*, **31,** 2026–2048.

Turner, J.S. (1979) *Buoyancy Effects in Fluids*. Cambridge University Press, Cambridge, 368 pp.

Woods, A.W., Sparks, R.S.J., Ritchie, L.J., Batey, J., Gladstone, C. and **Bursik, M.** (2002) The explosive decompression of a pressurised volcanic dome: the 26 December 1997 collapse and explosion of Soufrière Hills Volcano, Montserrat. In: *The Eruption of the Soufrière Hills Volcano, Montserrat, from 1995 to 1999* (Eds T.H. Druitt and B.P. Kokelaar), *Geol. Soc. London Mem.*, **21,** 457–465.

Manuscript received 27 March 2002; revision accepted 17 March 2004.